Microchimica Acta (2022) 189: 287
https://doi.org/10.1007/s00604-022-05357-8

ORIGINAL PAPER

SARS-CoV-2 virus label-free electrochemical nanohybrid MIP-aptasensor based on $Ni_3(BTC)_2$ MOF as a high-performance surface substrate

Zeinab Rahmati[1] · **Mahmoud Roushani**[1]

Received: 7 January 2022 / Accepted: 24 May 2022 / Published online: 19 July 2022

Abstract

A dual recognition biosensor was developed via introducing aptamer strings and molecular imprinting polymer (MIP) for the selective detection of intact SARS-CoV-2 virus based on screen printed carbon electrode (SPCE) modified with nickel-benzene tricarboxylic acid-metal–organic framework ($Ni_3(BTC)_2$ MOF) synthesized by in situ growth method, SARS-CoV-2 S protein-specific amino-aptamer and electropolymerization of dopamine (ePDA). The proposed biosensor showed an excellent linear relationship between charge transfer resistance (R_{ct}) and increase in virus concentration in the range 10 to 10^8 plaque-forming units/mL (PFU/mL) with a low detection limit of 3.3 ± 0.04 PFU/mL and response time of 20 min. Compared with single-element sensors (aptamer or MIP), it showed higher selectivity for the SARS-CoV-2 virus and facilitated detection in real samples.

Keywords SARS-CoV-2, covid 19 · In situ $Ni_3(BTC)_2$ MOF · Aptamer · Molecularly imprinted polymer · Electrochemical biosensor

Introduction

Modification of electrode surfaces with biomolecules such as aptamers, antibodies, enzymes, etc., to design electrochemical biosensors has constituted much research in recent years, and it has a very good perspective as the next-generation detection strategy for point-of-care testing [1–4]. Among the attractive properties of electrochemical biosensors is their innate high sensitivity, simplicity, cost effectiveness, small sample amount requirement, high selectivity, real-time monitoring, low detection limits, amenability to miniaturization, fast response times, etc., which has led to their potential application in various fields such as food control, environmental monitoring, drug discovery, medical diagnosis, forensics, and biomedical research, etc. [5–17]. Aptamers, specific sequences of nucleic acids, and ideal recognition elements in biosensors have three-dimensional binding sites which are synthesized artificially by the in vitro, and the ligand evolution and also the exponential enrichment (SELEX) process. Aptamers have gained much interest as synthetic antibodies in recent years among the various biomolecules used to make biosensor layers, and can be used to identify a wide range of targets, from small molecules to intact cells [18–21]. However, the performance of aptamers may be affected by acidic solvents, some nuclease enzymes at high temperatures [22, 23]. MIPs, tailored sensing materials that produced using template-sacrificing synthetic method, have attracted much attention as promising candidates for biological molecular recognition. The advantages of MIPs are long-term durability, high strength, high detection ability, chemical and thermal stability, direct and cost-effective synthesis, which allows them to be used in a wide range of applications, including biosensors, chemical reaction catalysis, drug delivery, separation, and so on [24–26]. Nevertheless, these synthetic receptors have disadvantages despite their desirable properties such as weak binding affinity and slow mass transfer which limit their use in selective detection of real samples in electrochemical sensors [27, 28]. A potentially promising idea to overcome the shortcomings of aptamer receptors and MIP is to integrate aptamers into MIP polymer scaffolds and

✉ Mahmoud Roushani
m.roushani@ilam.ac.ir; mahmoudroushani@yahoo.com

[1] Department of Chemistry, Faculty of Sciences, Ilam University, P.O. Box 69315-516, Ilam, Iran

develop a dual recognition strategy that leads to the development of a MIP-aptamer hybrid bioreceptors with high specificity and improved sensitivity as well as overcome the challenges of protein imprinting [28].

Moreover, effective stabilization of biomolecules as receptors on the electrodes surface so that their biological activity is fully preserved, as well as increasing the sensitivity of the assay, is an important challenge for the development of efficient and long-term operational stability biosensors [29–35]. Recently, noteworthy advances in nanoscience and nanotechnology have opened new horizons in the design of electrochemical biosensors. The design and engineering of the electrode surface and the concurrent use of the benefits of electrochemical methods and nanostructures have greatly improved the sensitivity and analytical power of electrochemical biosensors [11, 17, 36, 37].

In this regard, to study biosensor substrates with comprehensive properties such as high level for biomolecule stabilization, biocompatibility and high stability, efforts have been made to develop new substrates based on metal – organic frameworks (MOFs) [38, 39]. MOFs, also known as porous coordinate polymers (PCPs), are a class of highly ordered inorganic–organic hybrid materials with ordered structure and possess designable that have been widely used in a variety of fields, including sensors, separation, drug delivery, catalysis, supercapacitors, batteries, gas-separation and storage, and more [40–47]. Notable advantages of MOFs include large specific surface area, ultrahigh porosity, thermal and chemical stability, and good electrochemical activity [48]. To take advantage of the promising benefits of MOFs in the design of biosensors, a thin layer of it must be placed on the surface of the electrode to stabilize the biomolecules. Various methods have been developed to modify the electrode surface with MOF, including: self-assembled monolayer, microwave-induced, seeded growth, solvothermal, liquid epitaxy, evaporation-induced and in-situ growth [48–54]. Among these methods, the in-situ growth of MOF on the electrode surface is an attractive technique due to its morphological controllability, fast and facile synthesis procedure. This synthesis method also prevents the aggregation of MOFs on the electrode surface, which leads to increased access to active sites and mechanical stability of the layers [40, 55]. To prepare the in-situ MOF, intermediate materials such as layered double hydroxides (LDHs) can be used as a self-sacrificing intermediate that can be easily and directly converted to MOF on the electrode surface. By placing the H_3BTC (1,3,5-benzene tricarboxylic acid) solution on the electrode surface modified with LDHs, the LDHs are converted to uniform MOF film through a rapid and easy acid–base reaction with H_3BTC without the use of any hazardous organic solvents or organic adhesives [40, 55].

LDHs are two-dimensional nanosheets with an interesting structure that are highly regarded by researchers in various fields of electrochemistry due to their attractive properties such as ease of preparation, excellent electrochemical activity, great physical stability, natural abundance, and cost-effectiveness [40, 55, 56]. They can be synthesized only by applying a constant negative potential through a simple electrodeposition method on the surface of the electrode in the presence of a solution containing desired metal ions.

Research on the direct in situ growth MOFs has focused on the applications of electrocatalysis and capacitors. Shahrokhian group presented in situ growth MOFs of Cu MOF, CoZn MOF, and NiCo MOFs for glucose measurement [40, 55, 56]. Huang et al. used NiCo MOF nanosheets obtained from template-controlled in-situ growth on Ni foam for high performance asymmetric supercapacitors [57]. However, as far as we know, this technique has not been used to develop biosensors for loading biomolecules and to improve the properties of electrochemical biosensors.

Various nickel-based nanoparticles are of great interest for the development of various biosensors because, in addition to good conductivity, low cost and electro-inactivity in physiological pH solutions, they have robust interactions with biological molecules and due to their high biocompatibility, they are able to maintain the biological activity of biomolecules [4, 17].

In this work, Ni-LDH was first synthesized on the SPCE surface by electrodeposition method, then, by pouring the H_3BTC on the surface, the Ni-LDH became directly Ni-BTC MOF. Ni-BTC MOF was used as a suitable substrate with a high surface area for covalent immobilization of amino-functionalized aptamer as biological receptor elements which leads to more loading of the aptamer[SARS-CoV-2 virus] complex and therefore improves the sensitivity and electrochemical signal to determine the intact SARS-CoV-2 virus. By attaching the aptamer[SARS-CoV-2 virus] complex to the modified electrode surface as well as the electropolymerization of dopamine on it and then removing the SARS-CoV-2 virus as template, the nanohybrid aptamer[SARS-CoV-2 virus]-MIP was obtained. The polymer matrix traps the SARS-CoV-2 virus and its associated aptamers so that the aptamer and SARS-CoV-2 virus can interact with the polymer scaffold units. Thus, the polymer matrix not only acts as a protective scaffold, but also encloses aptamer molecules. The interaction of the SARS-CoV-2 virus and cavity of the MIP-aptamer nanohybrid leads to a change in the R_{ct} between the $[Fe(CN)_6]^{3-/4-}$ as redox probe and the electrode surface. The proposed electrochemical sensor demonstrated excellent selectivity, ultrasensitive and repeatable SARS-CoV-2 virus detection with a detection limit of 3.3 ± 0.04 PFU/mL and the possibility of application in actual samples.

Experimental section

Materials

The SARS-CoV-2 spike glycoprotein–specific aptamers were custom-synthesized by Bioneer (South Korea). Besides, the sequences are given as follows [58, 59]: 5′-NH_2-TCGCTCTTTCCGCTTCTTCGCGGTCATTGTGCATCC TGACTGACCCTAAGGTGCGAACATCGCCCGCGTAAG TCCGTGTGTGCGAA-3′.

Analytical grade of disodium hydrogen phosphate (Na_2HPO_4), sodium hydroxide (NaOH), sodium chloride (NaCl), 1,3,5-benzene tricarboxylic acid ($C_9H_6O_6$, H_3BTC), potassium nitrate (KNO_3), nickel nitrate hexahydrate ($Ni(NO_3)_2{\cdot}6H_2O$), monosodium dihydrogen phosphate (NaH_2PO_4), ethanol (C_2H_6O), and all other reagents were bought from Sigma-Aldrich or Merck and they were used sans additional purification. A redox probe was used which was prepared as a 0.01 M phosphate-buffered solutions (PBS) with pH = 7.4 containing $K_3Fe(CN)_6/K_4Fe(CN)_6$ (5 mM) in a 1 to 1 ratio and the all experiments were performed at room temperature.

Instruments and electrodes

The electrochemical investigations were recorded using a μ-Autolab type III/FRA2 (Eco Chemie B.V., Ultrecht, The Netherlands) instrument equipped with NOVA software. The SPCE with 2 mm in diameter (bought from Dropsens (Spain)) was applied as a three-electrode planar based on a graphite working electrode, silver pseudo-reference electrode and a carbon counter electrode. In order to investigate surface morphology, a MIRA3 TESCAN-LMU field-emission scanning electron microscope (FESEM) was applied which was then equipped with an EDS probe. In order to measure the pH, the Metrohm pH meter (model 780 pH/mV meters) was applied.

$Ni_3(BTC)_2$ MOF@SPCE fabrication

Before modification of SPCE with $Ni_3(BTC)_2$ MOF, its surface was cleaned by electrochemical method. For this purpose, 10 μL of NaOH solution (0.1 M) was dropped onto the SPCE as working electrode surface and a sweeping potential was applied during 10 consecutive cycles and finally, the electrode surface was then washed with distilled water and dried by nitrogen gas. Next, with the aim of formation of a thin layer of the $Ni(OH)_2$ for the subsequent conversion to $Ni_3(BTC)_2$ MOF, a drop of solution containing 0.01 M of $Ni(NO_3)_2.6H_2O$, and 0.02 M of KNO_3 was dropped on the clean SPCE surface and a constant cathode potential of − 1.1 V was applied to it for 300 s. In the next step, for in-situ conversion of $Ni(OH)_2$ NPs@SPCE to $Ni_3(BTC)_2$ MOF@SPCE, a drop of ethanolic solution containing 100 mg of H_3BTC in 1.8 mL of absolute ethanol and 4.7 mL of deionized water, as the organic linker, was placed on the as-prepared $Ni(OH)_2$ NPs@SPCE for 20 min. At the end, the modified electrode was washed with distilled water to remove excess MOFs from its surface.

Construction of the MIP-aptamer nanohybrid

Scheme 1 shows the steps of fabrication of MIP-aptamer nanohybrid. The in-situ $Ni_3(BTC)_2$ MOF layer on the SPCE surface was used as a substrate to load the amino-aptamer strings. First, in order to prepare the aptamer[SARS-CoV-2 virus] complex, the 100 μL of 10 μM SARS-CoV-2–specific amino-aptamer with 10^8 PFU/mL SARS-CoV-2 virus was incubated for 1 h at 37 °C in buffer solution with pH = 7.4 under slow stirring. Then, a drop of the obtained solution was incubated onto the surface of $Ni_3(BTC)_2$ MOF@SPCE for 1 h to covalent-immobilize them, through the amine groups in the end of aptamer string on $Ni_3(BTC)_2$ MOF@SPCE surface. Before performing the next step, to saturate possible free aptamer strings, a drop of 10^5 PFU/mL of SARS-CoV-2 virus was placed on the surface of modified electrode for 15 min. Next, with the aim of MIP-aptamer nanohybrid preparation, MIP formation was performed by ePDA on the aptamer[SARS-CoV-2 virus] complex/$Ni_3(BTC)_2$ MOF@SPCE. In this sense, 10 μM of PBS (pH 7.4) comprising 5 mM dopamine was placed on the electrode surface and 14 continuous cycles was applied in the potential range of − 0.5 to 0.5 V at a scan rate 50 $mV.s^{-1}$. Then, the viruses were removed from the ePDA-aptamer[SARS-CoV-2 virus]/$Ni_3(BTC)_2$ MOF@SPCE surface by washing the electrode under stirring for 15 min in the NaCl solution (0.1 M). In order to confirm the efficiency of the proposed strategy and control the conditions, a non-molecularly imprinted polymer (NIP-aptamer) was prepared as a control electrode according to the same method but without washing process, that due to the lack of washing process, no cavities are created on the electrode surface. The resulting modified electrode was named MIP-aptamer nanohybrid/$Ni_3(BTC)_2$ MOF@SPCE. After each step of electrode surface modification, the surface of electrode was washed with DI water to remove unbound molecules and dried under N_2 gas.

Analysis protocol

The samples were analyzed by EIS technique as the measuring technique. Besides, in order to investigate their repeatability, each sample was tested three times. The real patients and healthy individual samples, where the results are already confirmed using the standard PCR procedure, were provided

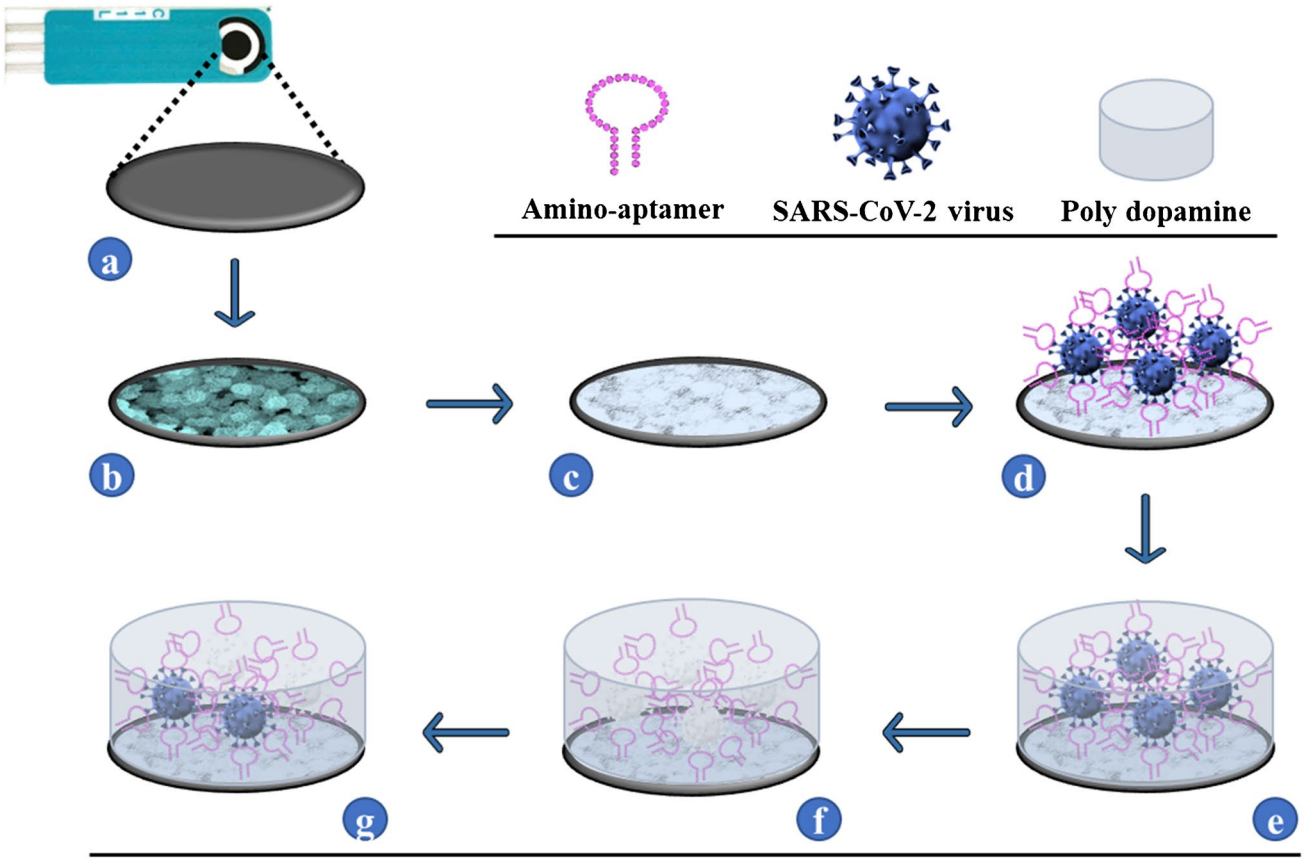

Scheme 1 Schematic illustration of the fabrication process of the aptasensor: (**a**) SPCE, (**b**) $Ni(OH)_2$@SPCE, (**c**) $Ni_3(BTC)_2$ MOF@SPCE, (**d**) aptamer[SARS-CoV-2 virus] complex/$Ni_3(BTC)_2$ MOF@SPCE, (**e**) ePDA/aptamer[SARS-CoV-2 virus] complex/$Ni_3(BTC)_2$ MOF@SPCE, (**f**) MIP-aptamer nanohybrid/$Ni_3(BTC)_2$ MOF@SPCE, and (**g**) SARS-CoV-2 virus/MIP-aptamer nanohybrid/$Ni_3(BTC)_2$ MOF@SPCE

from a clinical laboratory. The nasopharyngeal swab samples in viral transport medium (VTM) were inactivated by being heated at 100 ℃ for 10 min and were stored in the freezer for further use. The samples were diluted ten times with PBS and, then, tested by MIP-aptamer nanohybrid.

For different sample matrices including saliva and VTM, various concentrations of SARS-CoV-2 virus were added to these samples and, then, a drop of each solution was separately drooped on the MIP-aptamer nanohybrid independent from the others. Besides, the standard addition method was adopted for this purpose and, finally, recoveries of different concentrations of SARS-CoV-2 virus were also investigated.

Results and discussion

The morphological characterization of $Ni(OH)_2$ NPs@SPCE and $Ni_3(BTC)_2$MOF

The morphological properties of as-made metal hydroxides and MOFs were evaluated using FE-SEM technique. As shown in Fig. 1(d–f), $Ni(OH)_2$ mediators have a nanospheric morphology that is uniformly distributed on the electrode surface. In addition, Fig. 1(g–i) shows FE-SEM images of modified SPCE after immersion in the BTC solution and formation of $Ni_3(BTC)_2$ MOF@SPCE. As can be seen, these materials have different morphology that grows on the electrode surface. It is clear that there is a suitable substrate that is suitable for further loading of aptamer. Moreover, the EDX spectrum clearly indicates the attendance of Ni, C, and O in $Ni_3(BTC)_2$ MOF (Fig. 1j). Also, elemental mapping illustrates the uniform dispersal of elements in the structure (Fig. 1(k–n)).

Electrochemical characterization of the MIP-aptamer nanohybrid

The step-by-step MIP-aptamer nanohybrid fabrication process was characterized via electrochemical impedance spectroscopy (EIS) as a sensitive electrochemical technique, in redox probe solution at a potential of 0.23 V. Figure 2A displays the Nyquist plots that the observed semicircle portion

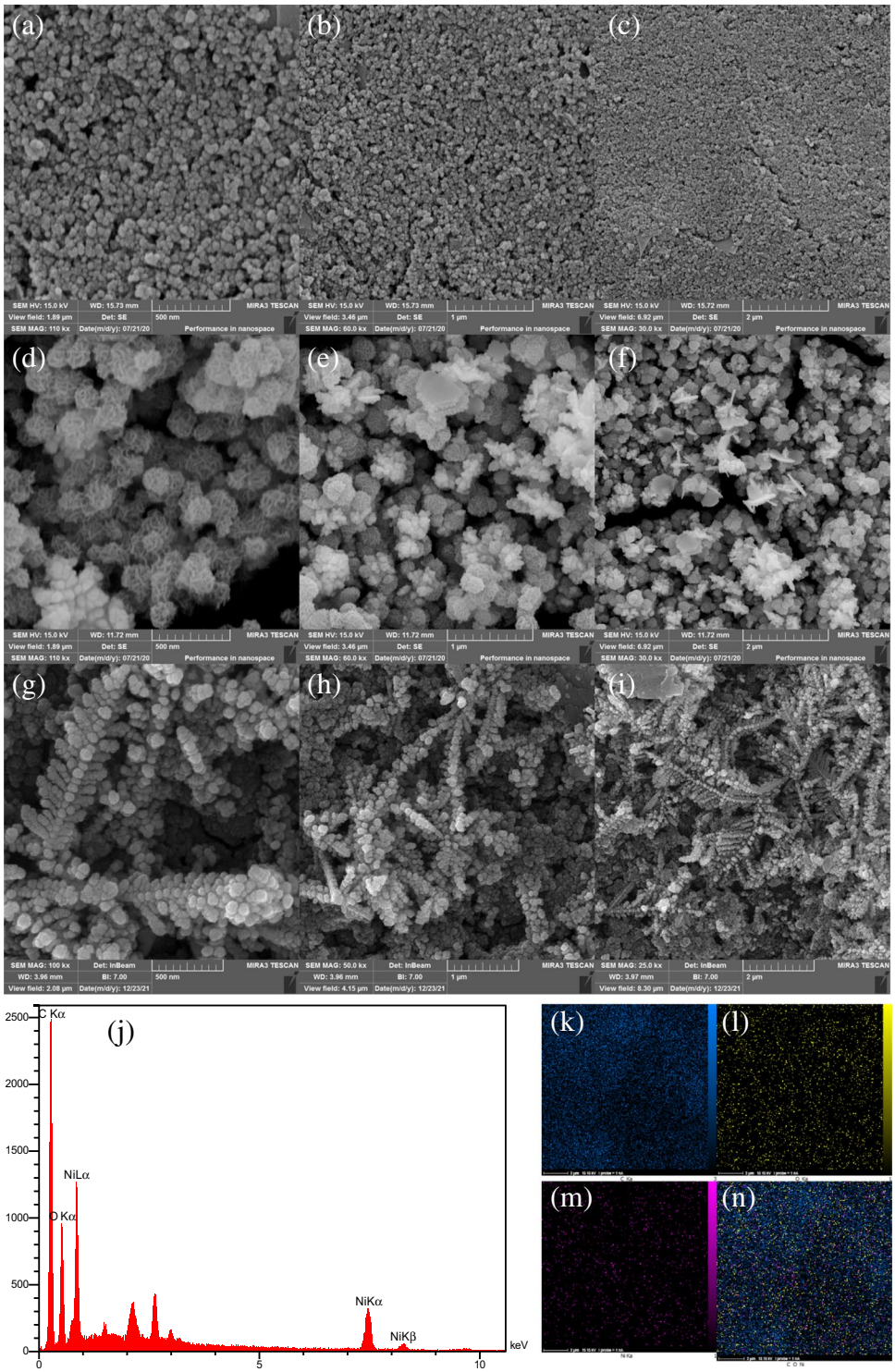

Fig. 1 The FESEM images of (**a**–**c**) SPCE, (**d**–**f**) $Ni(OH)_2$ NPs@SPCE and (**g**–**i**) $Ni_3(BTC)_2$ MOF@SPCE, and (**j**–**n**) the EDX spectrum and EDS mapping of $Ni_3(BTC)_2$ MOF@SPCE

at high frequencies is associated with the R_{ct}, and the linear part at low frequencies is associated wih the finite propagation process. First, a quite small resistance to electron-transfer was observed for the bare electrode which indicates its good conductivity and direct electrons transfer on the electrode surface (R_{ct} = 0.35 kΩ, curve "a"). The diameter of semicircle increased after $Ni_3(BTC)_2$ MOF was embellished on SPCE surface (R_{ct} = 0.88 kΩ, curve "b"), due to the repulsion force between the $Ni_3(BTC)_2$ MOF, which has a negative charge and the anionic redox probe species that lead to increased R_{ct}. As expected, R_{ct} increased significantly after immobilization of the aptamer[SARS-CoV-2 virus] complex on the modified electrode surface, due to the creation of a steric hindrance at the electrode surface (R_{ct} = 4.5

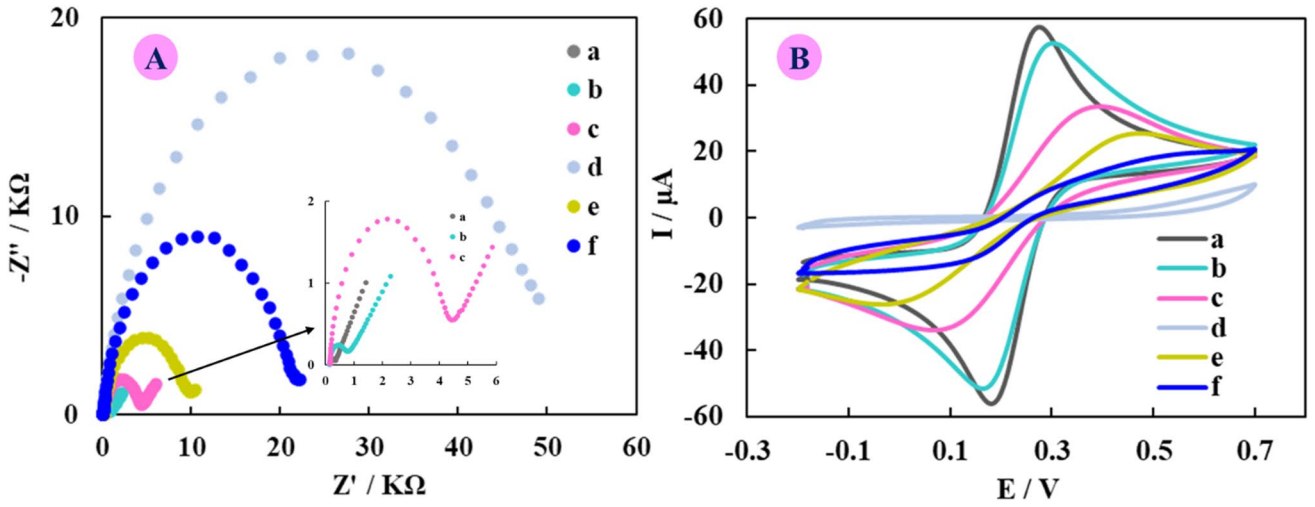

Fig. 2 The obtained (**A**) Nyquist curves, and (**B**) CV curves for each step of the modified electrode preparation in PBS with pH = 7.4 containing $K_3Fe(CN)_6/K_4Fe(CN)_6$ (5 mM) in a 1 to 1 ratio, (a) SPCE, (b) $Ni_3(BTC)_2$ MOF@SPCE, (c) aptamer[SARS-CoV-2 virus] complex/$Ni_3(BTC)_2$ MOF@SPCE, (d) ePDA/aptamer[SARS-CoV-2 virus] complex/$Ni_3(BTC)_2$ MOF@SPCE, (e) MIP-aptamer nanohybrid/$Ni_3(BTC)_2$ MOF@SPCE, and (f) SARS-CoV-2 virus/MIP-aptamer nanohybrid/$Ni_3(BTC)_2$ MOF@SPCE

kΩ, curve "c"). A significant increase in R_{ct} was observed after electropolymerization of electrode surface with dopamine (R_{ct} = 50 kΩ, curve "d"), as expected that can block the electron-transfer of the redox probe at the electrode surface. By means of washing the electrode surface with salt solution, a decrease in R_{ct} value was observed (R_{ct} = 10.1 kΩ, curve "e"), which was due to the reduction of steric/conformational restriction and better electron transfer after the removal of SARS-CoV-2 virus from the aptamer[SARS-CoV-2 virus] complex and the generation of the template holes. Correspondingly, when incubating with 10^3 PFU/mL of SARS-CoV-2 virus, R_{ct} increased obviously (R_{ct} = 22.2 kΩ, curve "f"), due to the trapped SARS-CoV-2 virus into the cavities on the electrode surface and the greater hindrance in the electron transfer.

Further, the electrochemical behaviors each step of electrode modification were investigated using cyclic voltammetry (CV) responses in redox probe solution. As can be seen in Fig. 2B, the resulting redox probe current has decreased after the modification on the surface of electrode in each step which was in a similar trend to that observed for the EIS response. These observations from both of these electrochemical measurements showed that all molecular events occurred successfully on the electrode surface.

Optimization of experimental conditions

Toward ensuring optimum performance, effects of some experimental parameters on response of the proposed MIP-aptamer nanohybrid were investigated, for example pH, incubation time of target. For this purpose, EIS response in redox probe solution was used. Since aptamer strings and SARS-CoV-2 virus are biological molecules, we need a neutral medium to prevent their degradation and ensure their satisfactory performance, so the pH of all solutions was set to 7.4.

With the aim of study, the effect of the incubation time of aptamer[SARS-CoV-2 virus] complex on the proposed biosensor performance, the EIS experiments in the redox probe solution were used. Fig. S1A shows a rapid increase in R_{ct} value from 10 min to 2 h, and when the incubation time was more than 1 h, a plateau was observed, indicating modified electrode surface saturation with the maximum number of aptamer [SARS-CoV-2 virus] complex.

The elution time of the template was optimized by EIS responses in redox probe solution and the maximum response was obtained in 15 min (Fig. S1B).

The connection time between SARS-CoV-2 virus and nanohybrid was optimized by EIS responses in redox probe solution to obtain the highest electrochemical response of the proposed biosensor. Fig. S1C shows that the growth of R_{ct} also increased with increasing incubation time, reaching a maximum in 15 min, after which time changed negligibility, indicating that 15 min was sufficient for detection of SARS-CoV-2 virus.

Analytical performance of the MIP-aptamer nanohybrid

The analytical performance of MIP-aptamer nanohybrid based on $Ni_3(BTC)_2$ MOF was examined by measuring EIS response to the SARS-CoV-2 virus at a series of concentrations under the optimized experimental conditions. Figure 3 presents that the R_{ct} value increases gradually with

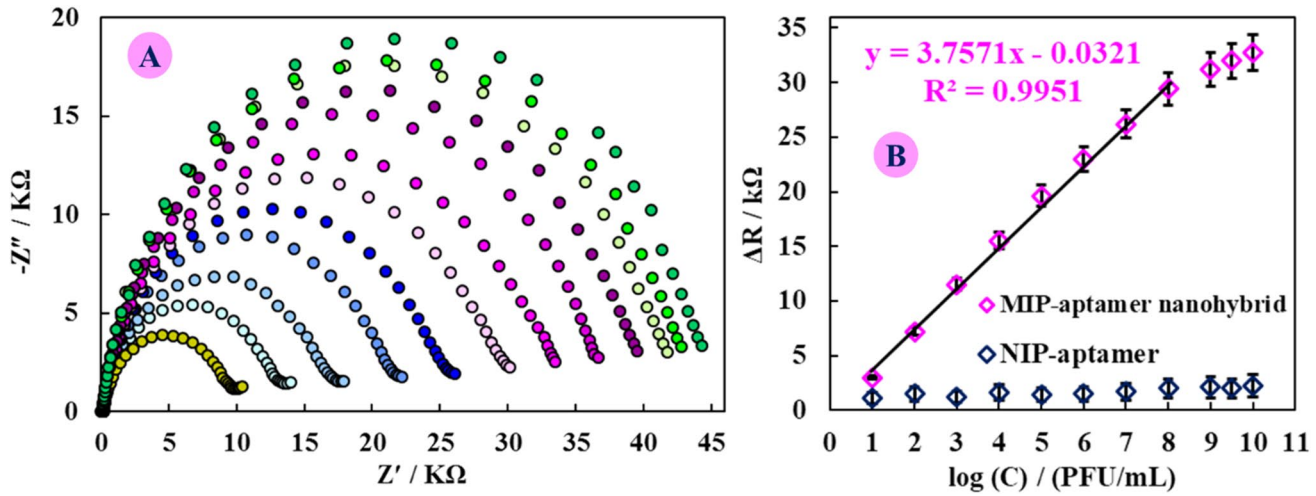

Fig. 3 **A** The EIS response of the MIP-aptamer nanohybrid after incubating with different SARS-CoV-2 virus with concentrations of 10 to 10^8 PFU/mL and 10^9 to $10.^{10}$ PFU/mL (out of the linear range) ($n = 3$) in PBS with pH = 7.4 containing $K_3Fe(CN)_6/K_4Fe(CN)_6$ (5 mM) in a 1 to 1 ratio. **B** Calibration curve of EIS response related to MIP-aptamer nanohybrid vs log $C_{SARS\text{-}CoV\text{-}2}$ virus (PFU/mL)

the increasing SARS-CoV-2 virus concentration. Increasing the SARS-CoV-2 virus concentration leads to the formation of more SARS-CoV-2 virus–aptamer complex on the MIP-aptamer nanohybrid surface and as a stationary blocking film causes procrastination of the redox probe to reach the electrode surface. The calibration curve was plotted using EIS response versus logarithmic scale of SARS-CoV-2 virus concentration in the range from 10 to 10^8 PFU/mL with a regression equation of $\Delta R\ (k\Omega) = 3.7571 \log C\ (PFU/mL) - 0.0321$ ($R^2 = 0.9951$) and the detection limit is 3.3 ± 0.04 PFU/mL (S/N = 3). The good sensitivity of the MIP-aptamer nanohybrid $Ni_3(BTC)_2$ MOF@SPCE substrate possibly credited to the high surface area and biocompatible environment of $Ni_3(BTC)_2$ MOF@SPCE, which increases the loading of aptamer[SARS-CoV-2 virus] complex by covalent bonding as well as, the presence of bonded cavities according to the shape, size, and functional groups according to the SARS-CoV-2 virus, would increase the sensitivity of electrochemical measurement. Also, for NIP-aptamer, due to the absence of empty cavities in the electrode surface with incubation of different concentrations of SARS-CoV-2 virus, no significant response was observed. Also, the performance of the prepared MIP-aptamer nanohybrid was compared with some previous reports. From Table S1, it was found that the LOD and assay reaction time of the MIP-aptamer nanohybrid are similar or better than some reported methods.

Other sensing performances of the proposed MIP-aptamer nanohybrid

The selectivity of the MIP-aptamer nanohybrid was investigated as an essential performance of biosensors. The proposed biosensor was incubated with 10^5 PFU/mL of SARS-CoV-2 virus and several potential types of possible interferers such as SARS-CoV, MERS-CoV, influenza A H_1N_1 and influenza A H_3N_2 and PBS under the same condition, respectively. As shown in Fig. S2A, the proposed biosensor exhibited an intense response to the target, while no significant response was observed for off-target species. The results are indicating that this biosensor had excellent selectivity.

The regeneration efficiency of MIP-aptamer nanohybrid was also investigated. The MIP-aptamer nanohybrid was regenerated by incubating the electrode with washing solution and rinsed off with PBS. The EIS response of MIP-aptamer nanohybrid was measured after each regeneration step that shows that after five runs of regeneration of sensor, the signals of the MIP-aptamer nanohybrid were almost recovered (Fig. S2B).

The reproducibility of the proposed biosensor was studied using the fabricated five independent electrodes and interacted with 10^5 PFU/mL of SARS-CoV-2 virus under the same conditions. Then, the EIS responses were recorded in redox probe solution (Fig. S2C). ΔR_{ct} obtained from EIS signals shows a relative standard deviation (RSD) of 4.2% that confirms the satisfactory reproducibility of the proposed biosensor.

Moreover, regarding the five repeated measurements of 10^5 PFU/mL of SARS-CoV-2 virus, the repeatability of the MIP-aptamer nanohybrid was evaluated. The obtained RSD value was 1.4% (Fig. S2D); confirming that the designed aptasensor had excellent repeatability.

Also, the long-term stability of the MIP-aptamer nanohybrid was evaluated by storing it at 4° C for 2 weeks. The ΔR_{ct} values obtained from the sensor do not show a significant change after 14 days, indicating the satisfied stability of the proposed biosensor (Fig. S2E).

Table 1 Measurement of SARS-CoV-2 virus in real samples with MIP-aptamer nanohybrid

Patients	PCR test	MIP-aptamer nanohybrid test	Patients	PCR test	MIP-aptamer nanohybrid test
#1	--	--	**#16**	+	+
#2	--	--	**#17**	+	+
#3	--	--	**#18**	+	+
#4	--	--	**#19**	+	+
#5	--	--	**#20**	+	+
#6	--	--	**#21**	+	+
#7	--	--	**#22**	+	+
#8	--	--	**#23**	+	+
#9	--	--	**#24**	+	+
#10	--	--	**#25**	+	+
#11	--	--	**#26**	+	+
#12	--	--	**#27**	+	+
#13	--	--	**#28**	+	+
#14	--	--	**#29**	+	+
#15	--	--	**#30**	+	+

The double exact molecular recognition property of the molecular imprinting polymers and aptamers led to the superb sensing properties. This satisfactory sensory function can be attributed to the fact that in the proposed method, while binding the target molecule to the aptamer, entrapment in the polydopamine polymer matrix is another effective factor for stabilizing the analyte at the electrode surface, and thus the stability and selectivity in this method is increased. In this regard, the EIS response of the MIP-aptamer nanohybrid/$Ni_3(BTC)_2$ MOF@SPCE, aptamer/$Ni_3(BTC)_2$ MOF@SPCE and MIP/$Ni_3(BTC)_2$ MOF@SPCE, aptamer/$Ni_3(BTC)_2$ MOF@SPCE with 10^5 PFU/mL of SARS-CoV-2 virus was also examined (Fig. S3). The obtained results showed that the hybrid detection system in MIP-aptamer nanohybrid/$Ni_3(BTC)_2$ MOF@SPCE had better sensitivity, selectivity, and detection efficiency recognition. In addition, this strategy to increase the sensitivity of the sensor has been used in several literature [22, 26, 29, 61, 62].

Application of the proposed MIP-aptamer nanohybrid in real samples

Potential of clinical application of the MIP-aptamer nanohybrid was assessed by diagnosis of SARS-CoV-2 virus in real samples of sick and healthy individuals in VTM previously confirmed by PCR. Each sample was tested with the proposed biosensor and measuring EIS in redox probe solution under optimal conditions. The results summarized in Table 1 showed that the MIP-aptamer nanohybrid was able to detect SARS-CoV-2 infection as benchmarked by PCR test with 100% sensitivity (positive percent agreement) and samples of healthy individuals with 100% specificity (negative percent agreement). These results showed that the MIP-aptamer nanohybrid was able to detect SARS-CoV-2 virus in actual clinical samples and can be used in real clinical samples.

Also, for feasibility of using the MIP-aptamer nanohybrid with the aim of quantitative detection of the SARS-CoV-2 virus in real sample, saliva and VTM samples spiked with SARS-CoV-2 virus were analyzed. The spiked samples were estimated using calibration curves, and the relevant data are summarized in Table S1. The recovery was from 98 to 104% and, also, the RSDs were found to be 4.2%. These results indicate that the MIP-aptamer nanohybrid can be used to quantitatively detect the SARS-CoV-2 virus in real samples with relatively good accuracy.

Conclusions

We offered a dual-recognition strategy based on a hybrid of MIP-aptamer for sensitive and selective diagnosis of SARS-CoV-2 virus using a disposable SPCE modified by in situ growth Ni-BTC MOF as a suitable substrate with a high surface area for covalent immobilization of amino-functionalized aptamer. The results showed that the strategy based on dual recognition system compared to single element sensors (aptamer or MIP), showed more selectivity than the SARS-CoV-2 virus and facilitated detection in real samples, which may be due to the presence bonded cavities in proportion to the shape, size, and functional groups according to the SARS-CoV-2 virus. This strategy led to the development of one of the most sensitive biosensors capable of detecting intact SARS-CoV-2 virus in real samples of sick and healthy individuals. The proposed biosensor showed advantages such as excellent selectivity, wide dynamic range, good precision, stability, and superior sensitivity. The proposed strategy could potentially be used to create sensitive and selective biosensors as a significant device for detecting other pathogens.

Supplementary Information The online version contains supplementary material available at https://doi.org/10.1007/s00604-022-05357-8.

Acknowledgements The authors would like to thank Ilam University for supporting this research work.

Declarations

Ethics approval and consent to participate All experimental protocols were approved by the Experimentation Ethics Committee of Ilam University of Medical Sciences (Code: IR. MEDILAM. REC.1399.210). The clinical samples were provided from a local clinical laboratory. Informed consent was obtained from all participants included in the study.

Conflict of interest The authors declare no competing interests.

References

1. Du Y, Dong S (2017) Nucleic acid biosensors: recent advances and perspectives. Anal Chem 89:189–215
2. Beitollahi H, Khalilzadeh MA, Tajik S et al (2020) Recent advances in applications of voltammetric sensors modified with ferrocene and its derivatives. ACS Omega 5:2049–2059
3. Rahmati Z, Roushani M, Hosseini H, Choobin H (2021) Electrochemical immunosensor with Cu 2 O nanocube coating for detection of SARS-CoV-2 spike protein. Microchim Acta 188:1–9
4. Rahmati Z, Roushani M, Hosseini H, Choobin H (2021) An electrochemical immunosensor using SARS-CoV-2 spike protein-nickel hydroxide nanoparticles bio-conjugate modified SPCE for ultrasensitive detection of SARS-CoV-2 antibodies. Microchem J 170:106718
5. Pourfarzad H, Shabani-Nooshabadi M, Ganjali MR (2020) High lithium anodic performance of reduced Sn particles on Co metal-organic frameworks for lithium-ion batteries with a long-cycle life. Compos Part B Eng 193:108008
6. Rahmati Z, Roushani M, Hosseini H (2020) Hierarchical hollow sea-urchin-like Ni–Co diselenide encapsulated in N-doped carbon networks as an advanced core-shell bifunctional electrocatalyst for fabrication of nonenzymatic glucose and hydrogen peroxide sensors. Sensors Actuators B Chem 324:128730
7. Wu W, Wu L, Wu H et al (2017) Sulphides of the cobalt doped Ni7S6 type for glucose, hydrogen peroxide and nitrite sensing platform. Sensors Actuators B Chem 250:224–232
8. Roushani M, Rahmati Z, Golchin M et al (2020) Electrochemical immunosensor for determination of Staphylococcus aureus bacteria by IgY immobilized on glassy carbon electrode with electrodeposited gold nanoparticles. Microchim Acta 187:567
9. Shen J, Li Y, Gu H et al (2014) Recent development of sandwich assay based on the nanobiotechnologies for proteins, nucleic acids, small molecules, and ions. Chem Rev 114:7631–7677
10. Mohankumar P, Ajayan J, Mohanraj T, Yasodharan R (2020) Recent developments in biosensors for healthcare and biomedical applications: a review. Measurement 167:108293
11. Rahmati Z, Roushani M, Hosseini H (2022) Hierarchical nickel hydroxide nanosheets grown on hollow nitrogen doped carbon nanoboxes as a high-performance surface substrate for alpha-fetoprotein cancer biomarkers electrochemical aptasensing. Talanta 237:122924. https://doi.org/10.1016/j.talanta.2021.122924
12. Khanmohammadi A, Aghaie A, Vahedi E et al (2020) Electrochemical biosensors for the detection of lung cancer biomarkers: a review. Talanta 206:120251
13. Yu X, Yang H, Huang X (2018) Novel method for structure–activity relationship of aptamer sequences for human prostate cancer. ACS Omega 3:10002–10007
14. Jauset-Rubio M, El-Shahawi MS, Bashammakh AS et al (2017) Advances in aptamers-based lateral flow assays. TrAC Trends Anal Chem 97:385–398
15. Nikhil B, Pawan J, Nello F, Pedro E (2016) Introduction to biosensors. Essays Biochem 60:1–8
16. Dhiman A, Kalra P, Bansal V et al (2017) Aptamer-based point-of-care diagnostic platforms. Sensors Actuators B Chem 246:535–553
17. Rahmati Z, Roushani M, Hosseini H (2021) Amorphous Ni(OH)2 nano-boxes as a high performance substrate for aptasensor application. Measurement 110649. https://doi.org/10.1016/j.measurement.2021.110649
18. Hedayati N, Taghdisi SM, Yazdian-Robati R et al (2021) Selection of DNA aptamers for tramadol through the systematic evolution of ligands by exponential enrichment method for fabrication of a sensitive fluorescent aptasensor based on graphene oxide. Spectrochim Acta Part A Mol Biomol Spectrosc 259:119840
19. Ye H, Qin B, Sun Y, Li J (2017) Electrochemical detection of VEGF165 lung cancer marker based on Au-Pd alloy assisted aptasenor. Int J Electrochem Sci 12:1818–1828
20. Tuerk C, Gold L (1990) Systematic evolution of ligands by exponential enrichment: RNA ligands to bacteriophage T4 DNA polymerase. Science 249:505–510
21. Kashefi-Kheyrabadi L, Mehrgardi MA, Wiechec E et al (2014) Ultrasensitive detection of human liver hepatocellular carcinoma cells using a label-free aptasensor. Anal Chem 86:4956–4960
22. Wang Z, Fang X, Sun N, Deng C (2020) A rational route to hybrid aptamer-molecularly imprinted magnetic nanoprobe for recognition of protein biomarkers in human serum. Anal Chim Acta 1128:1–10
23. Chang X, Zhang C, Lv C et al (2019) Construction of a multiple-aptamer-based DNA logic device on live cell membranes via associative toehold activation for accurate cancer cell identification. J Am Chem Soc 141:12738–12743
24. Nawaz N, Bakar NKA, Mahmud HNME, Jamaludin NS (2021) Molecularly imprinted polymers-based DNA biosensors. Anal Biochem 630:114328
25. Roushani M, Rahmati Z, Hoseini SJ, Fath RH (2019) Impedimetric ultrasensitive detection of chloramphenicol based on aptamer MIP using a glassy carbon electrode modified by 3-ampy-RGO and silver nanoparticle. Colloids Surfaces B Biointerfaces 183:110451
26. Roushani M, Zalpour N (2021) Impedimetric ultrasensitive detection of Trypsin based on hybrid aptamer-2DMIP using a glassy carbon electrode modified by nickel oxide nanoparticle. Microchem J 106955
27. Sajini T, Mathew B (2021) A brief overview of molecularly imprinted polymers: highlighting computational design, nano and photo-responsive imprinting. Talanta Open 4:100072
28. Tan J, Guo M, Tan L et al (2018) Highly efficient fluorescent QDs sensor for specific detection of protein through double recognition of hybrid aptamer-molecular imprinted polymers. Sensors Actuators B Chem 274:627–635
29. Negahdary M, Heli H (2018) Applications of nanoflowers in biomedicine. Recent Pat Nanotechnol 12:22–33
30. Mahmoudpour M, Ding S, Lyu Z et al (2021) Aptamer functionalized nanomaterials for biomedical applications: recent advances and new horizons. Nano Today 39:101177. https://doi.org/10.1016/j.nantod.2021.101177
31. Walcarius A, Minteer SD, Wang J et al (2013) Nanomaterials for bio-functionalized electrodes: recent trends. J Mater Chem B 1:4878–4908
32. Hasanzadeh M, Sahmani R, Solhi E et al (2018) Ultrasensitive immunoassay of carcinoma antigen 125 in untreated human plasma samples using gold nanoparticles with flower like morphology: a new platform in early stage diagnosis of ovarian cancer and efficient management. Int J Biol Macromol 119:913–925
33. Huang X, Zhu Y, Kianfar E (2021) Nano biosensors: properties, applications and electrochemical techniques. J Mater Res Technol 12:1649–1672. https://doi.org/10.1016/j.jmrt.2021.03.048
34. Liu M, Liu R, Chen W (2013) Graphene wrapped Cu2O nanocubes: non-enzymatic electrochemical sensors for the detection of glucose and hydrogen peroxide with enhanced stability. Biosens Bioelectron 45:206–212
35. Zhu C, Yang G, Li H et al (2015) Electrochemical sensors and biosensors based on nanomaterials and nanostructures. Anal Chem 87:230–249

36. Rahmati Z, Roushani M, Hosseini H (2021) Thionine functionalized hollow N-doped carbon nanoboxes: as a high-performance substrate for fabrication of label-free electrochemical aptasensor toward ultrasensitive detection of carcinoembryonic antigen. J Electroanal Chem 115858
37. Roushani M, Hosseini H, Hajinia Z, Rahmati Z (2021) Rationally designed of hollow nitrogen doped carbon nanotubes double shelled with hierarchical nickel hydroxide nanosheet as a high performance surface substrate for cortisol aptasensing. Electrochim Acta 388:138608
38. Song Y, Xu M, Liu X et al (2021) A label-free enrofloxacin electrochemical aptasensor constructed by a semiconducting CoNi-based metal–organic framework (MOF). Electrochim Acta 368:137609. https://doi.org/10.1016/j.electacta.2020.137609
39. Guo C, Su F, Song Y et al (2017) Aptamer-templated silver nanoclusters embedded in zirconium metal–organic framework for bifunctional electrochemical and SPR aptasensors toward carcinoembryonic antigen. ACS Appl Mater Interfaces 9:41188–41199
40. Ataei-Kachouei M, Shahrokhian S, Ezzati M (2021) Bimetallic CoZn-MOFs easily derived from CoZn-LDHs, as a suitable platform in fabrication of a non-enzymatic electrochemical sensor for detecting glucose in human fluids. Sensors Actuators B Chem 130254
41. Li J-R, Sculley J, Zhou H-C (2012) Metal–organic frameworks for separations. Chem Rev 112:869–932
42. Wuttke S, Lismont M, Escudero A et al (2017) Positioning metal-organic framework nanoparticles within the context of drug delivery–a comparison with mesoporous silica nanoparticles and dendrimers. Biomaterials 123:172–183
43. Lee J, Farha OK, Roberts J et al (2009) Metal–organic framework materials as catalysts. Chem Soc Rev 38:1450–1459
44. Choi KM, Jeong HM, Park JH et al (2014) Supercapacitors of nanocrystalline metal–organic frameworks. ACS Nano 8:7451–7457
45. Fang G, Zhou J, Liang C et al (2016) MOFs nanosheets derived porous metal oxide-coated three-dimensional substrates for lithium-ion battery applications. Nano Energy 26:57–65
46. Pramudya Y, Mendoza-Cortes JL (2016) Design principles for high H2 storage using chelation of abundant transition metals in covalent organic frameworks for 0–700 bar at 298 K. J Am Chem Soc 138:15204–15213
47. Ma T, Li H, Ma J-G, Cheng P (2020) Application of MOF-based materials in electrochemical sensing. Dalt Trans 49:17121–17129
48. Zhang S, Zhang Y, Baig F, Liu T-F (2021) Synthesis and applications of stable iron-based metal–organic framework materials. Cryst Growth Des 21:3100–3122
49. Biemmi E, Scherb C, Bein T (2007) Oriented growth of the metal organic framework Cu3 (BTC) 2 (H2O) 3⊙ x H2O tunable with functionalized self-assembled monolayers. J Am Chem Soc 129:8054–8055
50. Yoo Y, Jeong H-K (2008) Rapid fabrication of metal organic framework thin films using microwave-induced thermal deposition. Chem Commun 2441–2443
51. Falcaro P, Hill AJ, Nairn KM et al (2011) A new method to position and functionalize metal-organic framework crystals. Nat Commun 2:1–8
52. Rodenas T, Luz I, Prieto G et al (2015) Metal–organic framework nanosheets in polymer composite materials for gas separation. Nat Mater 14:48–55
53. Shekhah O, Wang H, Paradinas M et al (2009) Controlling interpenetration in metal–organic frameworks by liquid-phase epitaxy. Nat Mater 8:481–484
54. Ameloot R, Gobechiya E, Uji-i H et al (2010) Direct patterning of oriented metal–organic framework crystals via control over crystallization kinetics in clear precursor solutions. Adv Mater 22:2685–2688
55. Ezzati M, Shahrokhian S, Hosseini H (2020) In situ two-step preparation of 3D NiCo-BTC MOFs on a glassy carbon electrode and a graphitic screen printed electrode as nonenzymatic glucose-sensing platforms. ACS Sustain Chem Eng 8:14340–14352
56. Shahrokhian S, Sanati EK, Hosseini H (2019) Advanced on-site glucose sensing platform based on a new architecture of free-standing hollow Cu (OH) 2 nanotubes decorated with CoNi-LDH nanosheets on graphite screen-printed electrode. Nanoscale 11:12655–12671
57. Huang S, Shi X-R, Sun C et al (2022) Template-controlled in-situ growing of NiCo-MOF nanosheets on Ni foam with mixed linkers for high performance asymmetric supercapacitors. Appl Surf Sci 572:151344
58. Rahmati Z, Roushani M, Hosseini H, Choobin H (2022) label-free electrochemical aptasensor for rapid detection of SARS-CoV-2 spike glycoprotein based on the composite of Cu (OH) 2 nanorods arrays as a high-performance surface substrate. Bioelectrochemistry 108106
59. Kacherovsky N, Yang LF, Dang HV et al (2021) Discovery and characterization of spike N-terminal domain-binding aptamers for rapid SARS-CoV-2 detection. Angew Chemie 133:21381–21385
60. Roushani M, Rahmati Z, Farokhi S et al (2020) The development of an electrochemical nanoaptasensor to sensing chloramphenicol using a nanocomposite consisting of graphene oxide functionalized with (3-Aminopropyl) triethoxysilane and silver nanoparticles. Mater Sci Eng C 108:110388
61. Roushani M, Farokhi S, Rahmati Z (2022) Development of a dual-recognition strategy for the aflatoxin B1 detection based on a hybrid of aptamer-MIP using a Cu2O NCs/GCE. Microchem J 178:107328
62. Vasapollo G, Del SR, Mergola L et al (2011) Molecularly imprinted polymers: present and future prospective. Int J Mol Sci 12:5908–5945